

Selective flocculation of ultrafine hematite with sodium polyacrylate

Fusheng Niu ^{1,3}, Yuying Chen ¹, Jinxia Zhang ^{1,3}, Fei Liu ¹, Ziye Wang ²

¹ College of Mining Engineering, North China University of Science and Technology, Tangshan 063210, China

² GRINM Resources and Environment Tech. Co., Ltd, Beijing 100006, China

³ Collaborative Innovation Center of Green Development and Ecological Restoration of Mineral Resources, Tangshan 063210, China

Corresponding authors: kyky@ncst.edu.cn (Jinxia Zhang), wangziye@grinm.com (Ziye Wang)

Abstract: The separation of ultrafine hematite and kaolinite using classical flotation and magnetic separation techniques is challenging due to their very fine particle size, which easily contaminates the concentrate, resulting in low grades. This research examines the flocculation effects and mechanisms of sodium polyacrylate (PAAS) on hematite and kaolinite through flocculation experiments, particle size analysis, zeta potential measurements, FTIR, and XPS analysis. The flocculation tests indicated that with a PAAS dosage of 2.25 mg · L⁻¹, ultrafine hematite exhibited good flocculation, with the average particle size increasing from 2.59 μm to 42.88 μm, and the fractal dimension could reach 1.59. Changes in zeta potential and adsorption amount showed that at a PAAS dosage of 2.25 mg · L⁻¹, the zeta potential reached a peak of -3.53 mV, and the adsorption amount was 0.01 mg · g⁻¹. The adsorption isotherm fitting results suggested that PAAS adsorption on hematite and kaolinite follows the Langmuir equation more closely, with hematite demonstrating better PAAS adsorption properties. FTIR analysis showed that sodium polyacrylate was chemisorbed on the surface of hematite. It was determined by XPS analysis that Fe³⁺ on the hematite surface reacted with the reactive group -COO⁻ in sodium polyacrylate.

Keywords: sodium polyacrylate, ultrafine hematite, selective flocculation, kaolinite

1. Introduction

With the continuous development of human society and the persistent consumption of mineral resources, easily treatable mineral resources are becoming increasingly scarce, drawing more attention to the development and utilization of refractory mineral resources (Li et al., 2021; Zhang et al., 2023). Influenced by mineralization characteristics, refractory mineral resources often have low grades, ultrafine dissemination sizes, and complex composition (Zhu et al., 2022; Wang et al., 2023a). Clay minerals frequently coexist with metal ores, non-metal ores, and coal as associated gangue minerals (Mochizuki and Tsubouchi, 2019; Cui et al., 2020). During the flotation process, the ultrafine and hydrophilic nature of clay minerals allows them to easily cover the surface of valuable minerals due to their anisotropy (Bai et al., 2020), reducing the hydrophobicity of valuable minerals, hindering their contact with collectors and bubbles, thereby deteriorating the flotation performance (Zhu et al., 2019). Additionally, due to the extremely fine particle size of clay minerals, usually less than 10 μm, they tend to enter the froth flotation concentrate, significantly reducing the concentrate grade and flotation selectivity (Chen and Peng, 2018; Yang et al., 2019; Yu et al., 2020). The high aspect ratio and non-spherical particle characteristics of clay minerals result in complex rheological behavior of their suspensions, significantly increasing the viscosity of flotation pulp containing fine clay minerals, which further inhibits the flotation and recovery of target mineral particles (Farrokhpay et al., 2016; Li et al., 2016). Flocculating and covering clay minerals is a major technical challenge in the field of fine mineral separation (Wang et al., 2024). Enhancing the hydrophobicity of clay mineral interfaces and desorbing them from the target mineral interfaces are crucial to solving this problem.

The main technical bottlenecks in improving ultrafine particle flocculation flotation indicators lie in two aspects: on the one hand, the selectivity of flocculants. The interference of particles and target

mineral inclusions during the flocculation process is the main reason for unsatisfactory flocculation flotation indicators. If the molecular chain strength of the flocculant used is high and the flocs are dense, it is difficult to remove the wrapped impurity particles in subsequent operations (Warren, 1975; Forbes, 2011; Yin et al., 2011; Bai et al., 2023; Wang et al., 2023b; Yang et al., 2023). On the other hand, the serious loss of target minerals during the desliming operation results in high flotation tailings grades and low concentrate recovery rates, causing serious resource waste (Raju et al., 1991; Pascoe and Wills, 1994; Akdemir, 1997; Pavlovic and Brandao, 2003; Rulyov et al., 2009; Xie et al., 2024).

Starch is the most commonly used flocculant and depressant for hematite in iron ore flotation. In fact, different types of flocculants have been studied to improve the separation efficiency of hematite. Yang Cheng et al. found that in the dodecylamine collector system, polyethylene oxide (PEO) and starch can be used as selective flocculants for quartz and hematite, respectively, achieving the flotation separation of the two (Yang et al., 2022). Han et al. studied the selective flocculation of Fe (III)-XG complex on hematite and quartz, showing strong selective flocculation at pH 6, with sedimentation rates of 91.50% and 39.96%, respectively (Han et al., 2024). Hydroxyl groups are the only active groups in natural starch polymer chains and mainly adsorb through hydrogen bonding when interacting with minerals, showing poor selectivity. Therefore, using starch as a depressant gradually exposes many shortcomings, such as poor solubility, relatively large dosage, and difficulty in handling the separated products.

Sodium polyacrylate (PAAS) is an anionic polyelectrolyte that easily forms complexes with divalent metal ions, thus widely used in water treatment. In recent years, the application of PAAS in mineral processing has been increasing. Chen et al. found that sodium polyacrylate flocculates serpentine by interacting with Mg^{2+} on the serpentine surface, changing the dispersion state of serpentine particles, thereby effectively inhibiting serpentine particles (Chen et al., 2022). Cheng et al. showed that after flocculating with PAAS, the collector NaOL can adsorb on the surface of hematite, while the adsorption of PAAS on quartz inhibits the adsorption of NaOL on the quartz surface, significantly improving the floatability of fine hematite and achieving effective separation of fine hematite from fine quartz (Cheng et al., 2022).

In this paper, the effects of flocculant PAAS on the selective flocculation behavior of microfine-grained hematite and kaolinite were investigated by flocculation test, adsorption test, infrared spectroscopy, zeta potential test, and XPS analysis, and the selective mechanism was analyzed, which provides a theoretical basis for the selective flocculation of ultrafine hematite and kaolinite.

2. Materials and methods

2.1. Materials

The pure minerals used in the experiments mainly include molybdenite and kaolinite. The high-purity ultrafine hematite required for the experiments was obtained by regrinding and reselecting the spiral chute concentrate from a mineral processing plant in Hebei Province, China. The XRD analysis results are shown in Fig. 1. The kaolinite used in the experiments was sourced from Henan Province, and large particles were removed by wet sieving. The dried kaolinite samples were then sampled, and the XRD analysis results are shown in Fig. 2. Chemical analysis showed that the purity of hematite and kaolin was 98.63% and 99.12% respectively, and the content of TFe in hematite was 67.90.

Laser particle size analysis was conducted on the experimental raw materials, with the volume-weighted average particle sizes of hematite and kaolinite being 2.59 μm and 1.61 μm , respectively, as shown in Figs. 3 and 4.

The flocculant used in the test was 6000000g/mol of analytical grade sodium polyacrylate purchased from Macklin Biochemical Co., Ltd, Shanghai, China.

2.2. Flocculation effect characterization

The experimental raw materials were subjected to ultrasonic treatment for 30 minutes and then stirred at a speed of 800-900 r/min for 2 minutes using a magnetic stirrer. PAAS solution was then added to the beaker, and stirring continued for another 2 minutes to form flocs of hematite and kaolinite, which were then characterized.

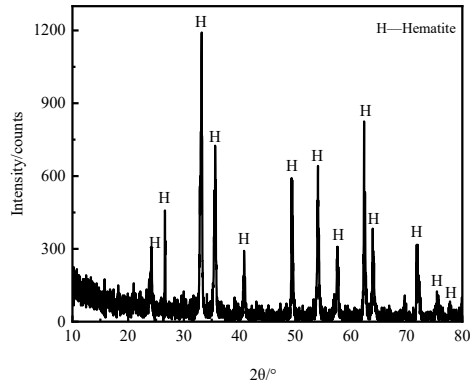


Fig. 1. XRD analysis results of hematite

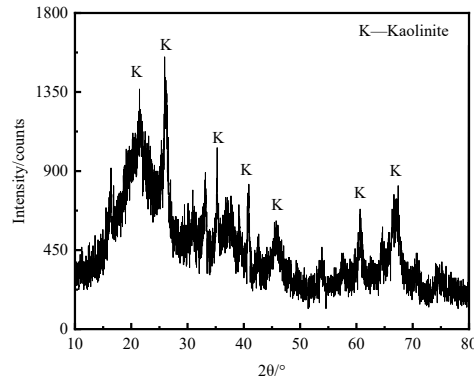


Fig. 2. XRD analysis results of kaolinite

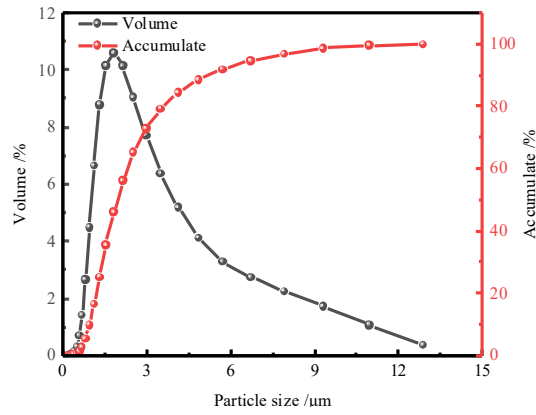


Fig. 3. Particle size analysis of hematite

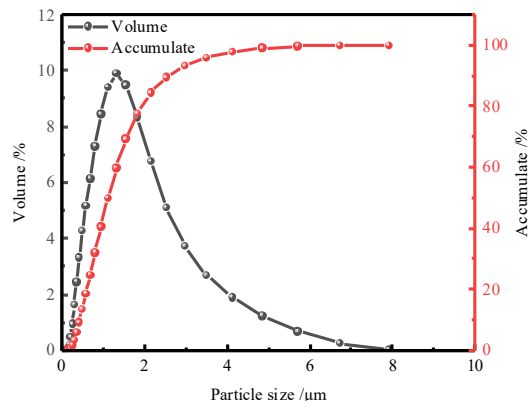


Fig. 4. Particle size analysis of kaolinite

2.2.1. Particle size and fractal dimension of flocs

The floc images were analyzed using Image-Pro Plus (IPP) image processing software to extract the floc size. The scale was set by photographing a ruler with different magnifications and setting the corresponding scale. The floc images were then processed with the appropriate scale, and the contours were extracted, with the results output in actual lengths. The image processing procedure is shown in Fig. 5. The analysis data of each contour were transferred to Excel for calculation.

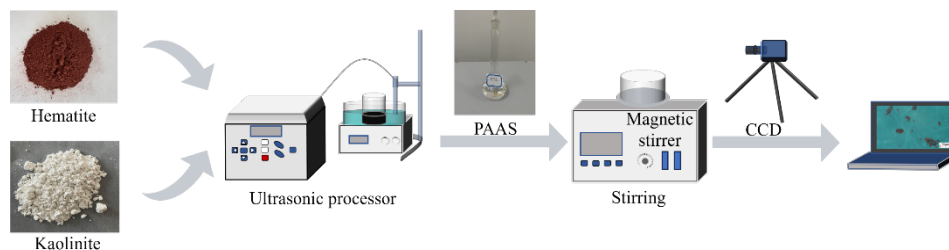


Fig. 5. Image-Pro Plus measures the particle size and area of the floc

Fractal dimensions of flocs can be used to analyze the porosity, permeability, density, and structure of flocs, representing the fractal irregularity and complexity. The denser the floc structure, the higher the fractal dimension (D_f). The relationship between the projected area and the maximum chord length of the flocs was fitted to obtain the two-dimensional fractal dimension, defined as:

$$S=BL^{D_f} \quad (1)$$

Taking the logarithm of both sides of the equation gives:

$$\ln S=\ln B+D_f \ln L \quad (2)$$

where S is the cross-sectional area, μm^2 ; B is the proportional constant, L is the longest distance (also called characteristic length), μm ; D_f is the fractal dimension.

The fractal dimension of the flocs was calculated by fitting a straight line to the double-logarithmic plot of the characteristic length and cross-sectional area and determining the slope of the line.

2.2.2 FTIR measurement

Samples under different conditions were dried at low temperatures and ground, then pressed into tablets using a KBr pellet press at a pressure of 2.0×10^5 MPa in an FW-4A powder tablet press machine. The FTIR spectra were measured on an FTIR-8400 Fourier transform infrared spectrometer in the range of $500\text{--}4000\text{ cm}^{-1}$.

2.2.3 Zeta potential measurement

The zeta potentials of and kaolinite and hematite at different dosages of PAAS were determined using a Zetasizer Mano zs90. The suspensions were stirred with a magnetic stirrer for 2 min. To accelerate the settling of large particles, the suspensions were centrifuged at 700 r/min for 8 min, and then a small amount of supernatant was added to the platinum electrode for measurement.

2.2.4 Determination of PAAS adsorption on mineral surfaces

Batch adsorption experiments were conducted using a Shimadzu TOC-L series total organic carbon analyzer with a liquid autosampler to quantify the PAAS adsorption on hematite and kaolinite during the flocculation process. The supernatant obtained after flocculation and sedimentation was used for these tests. Control samples were prepared by dissolving the same amount of polymer used in the flocculation tests in distilled water and centrifuging, ensuring that centrifugation did not alter the quantity of polymer present in the original samples. The TOC instrument was first calibrated to improve measurement accuracy. All standard solutions of IC (inorganic carbon) and TC (total carbon) ($0.0, 0.5, 1.0, 10, 20, 50\text{ mg}\cdot\text{L}^{-1}$) were freshly prepared from sodium bicarbonate, sodium carbonate, and potassium hydrogen phthalate obtained from Sigma Aldrich. The IC and TC calibration curves were plotted with

correlation coefficient values (R^2) > 0.99 (Figs. 6(a) and 6(b)). All adsorption tests were conducted at pH 7. The TOC value was determined by subtracting the IC amount from the TC amount.

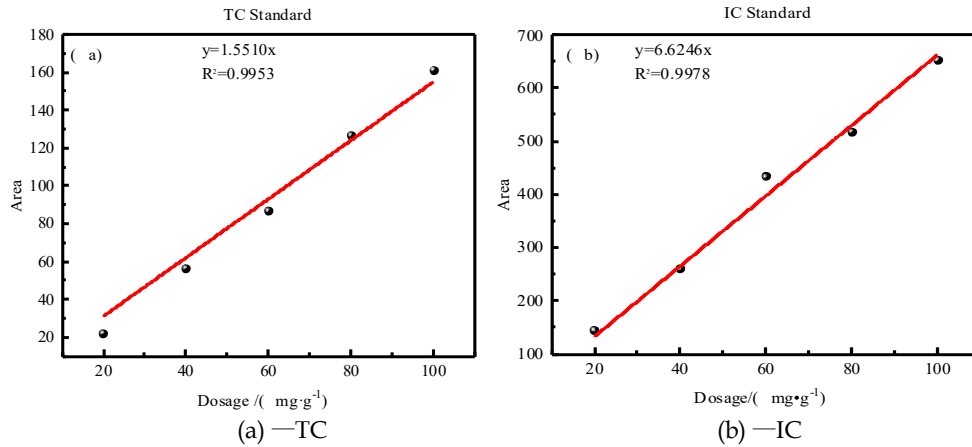


Fig. 6. TC (total carbon) and IC (inorganic carbon) standard curves

Assuming that the observed values of TOC are proportional to the concentration of PAAS, the difference in quantity before and after adsorption represents the amount adsorbed. The average adsorbed concentration of PAAS on hematite and kaolinite can be calculated using the mass balance equation, as shown in equation (3):

$$Q_e = \frac{(C_0 - C_e)V}{m} \quad (3)$$

where Q_e is the PAAS adsorption amount per unit mass of mineral at equilibrium, $\text{mg} \cdot \text{g}^{-1}$; C_0 is the initial PAAS concentration in the solution, $\text{mg} \cdot \text{L}^{-1}$; C_e is the PAAS concentration in the solution at equilibrium, $\text{mg} \cdot \text{L}^{-1}$; V is the total volume used, L; m is the mass of the mineral used, g.

The adsorption characteristics of reagents on minerals were described using two classic adsorption isotherm models: the Langmuir model and the Freundlich model. The model parameters were evaluated using linear least squares fitting. The Langmuir isotherm implies a finite number of equal adsorption sites, with no lateral interactions at these sites. The Langmuir equation is expressed as:

$$Q_e = \frac{Q_0 K_A C_e}{1 + K_A C_e} \quad (4)$$

Transforming the above equation gives the linearized Langmuir isotherm equation:

$$\frac{1}{Q_e} = \frac{1}{Q_0} + \frac{1}{K_A Q_0 C_e} \quad (5)$$

where Q_0 is the maximum adsorption capacity for a monolayer on the mineral, $\text{mg} \cdot \text{g}^{-1}$; C_e is the PAAS concentration in the solution at equilibrium, $\text{mg} \cdot \text{L}^{-1}$; K_A is the Langmuir adsorption constant, $\text{L} \cdot \text{g}^{-1}$.

Experimental data were fitted to the above equation by plotting $1/Q_e$ versus $1/C_e$.

The Freundlich isotherm, known as the earliest description of non-ideal and reversible adsorption, is not restricted to monolayer formation. The linearized Freundlich model equation used to estimate the adsorption intensity of PAAS on minerals is:

$$Q_e = K_F C_e^{\frac{1}{n}} \quad (6)$$

The linearized Freundlich isotherm equation is:

$$\ln Q_e = \ln K_F + \frac{1}{n} \ln C_e \quad (7)$$

where K_F is an adsorption constant related to temperature, the type of adsorbent and the specific surface area of the adsorbent; n is a dimensionless constant related to temperature and adsorption intensity.

Experimental data were fitted to the above equation by plotting $\ln Q_e$ versus $\ln C_e$.

2.2.5. XPS analysis

XPS analysis was performed using an ESCALAB Xi+ (Thermo Fischer, USA) under a vacuum of 8×10^{-10} Pa. The preparation of mineral samples for XPS analysis involved mixing 2.0 g of mineral samples

with 40 mL of distilled water in a beaker at a specified PAAS concentration, stirring for 2 minutes, then filtering by gravity, and vacuum drying at 60°C for XPS testing.

3. Results and discussion

3.1. Floc size and fractal dimension

The variation in floc size of hematite and kaolinite under different PAAS dosages is shown in Fig. 7, and the floc size and fractal dimension are shown in Fig. 8.

As can be seen from Fig. 7(a), with the increase of PAAS dosage, agglomeration occurs between hematite particles to form lumpy and long chain flocs, and mineral particles can be adsorbed on multiple flocculant molecular chains at the same time to form denser three-dimensional flocs. From Fig. 7(b), it can be seen that the size of kaolinite particles increased after the addition of PAAS, and the size of kaolinite particles did not change much by changing the dosage of PAAS. This shows that PAAS has a certain selectivity for hematite.

As can be seen from Fig. 8(a), the particle size and fractal dimension of hematite flocs increase with the increase of PAAS dosage. When the dosage of PAAS was 2.25 mg · L⁻¹, the particle size of hematite flocculation was larger, reaching 42.89 μm, and the fractal dimension of the flocculation was 1.59. When the dosage of PAAS was 4.25 mg · L⁻¹, the particle size of hematite floc reached the maximum value of 53.78 μm, and the fractal dimension of hematite floc reached the maximum value of 1.99, which was attributed to the fact that the increase of PAAS dosage favored the increase in hematite flocs' particle size and fractal dimension. The increase of PAAS dosage favored the agglomeration of mineral particles, and the flocs were gradually densified with increasing fractal dimension.

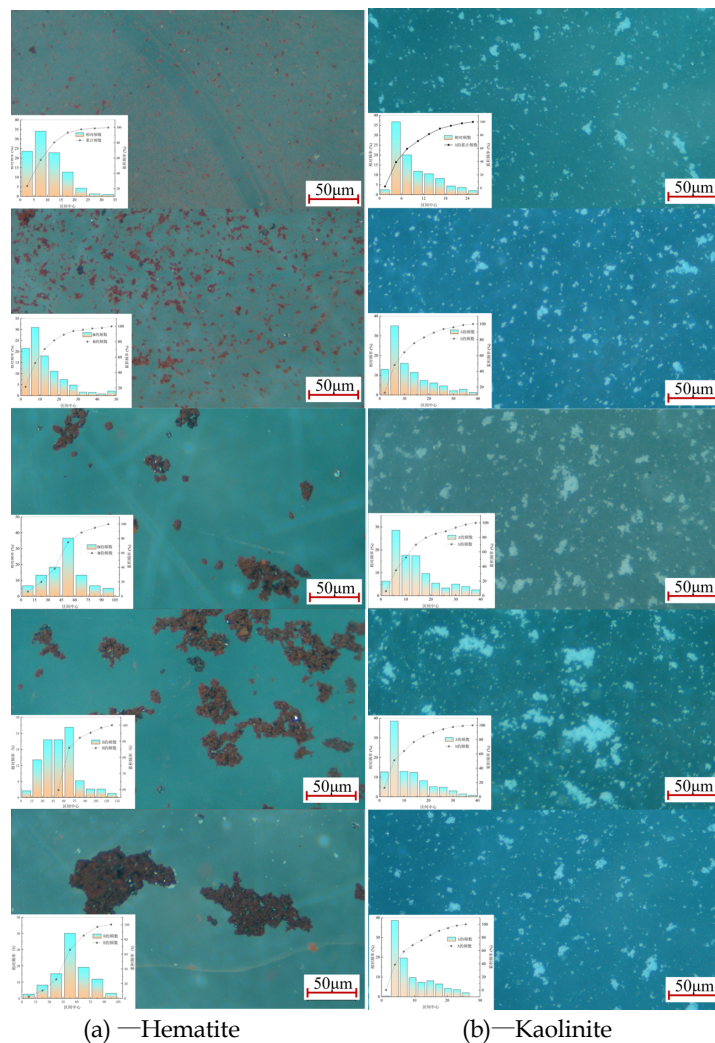


Fig. 7. Pictures of hematite and kaolinite flocs at different PAAS dosages

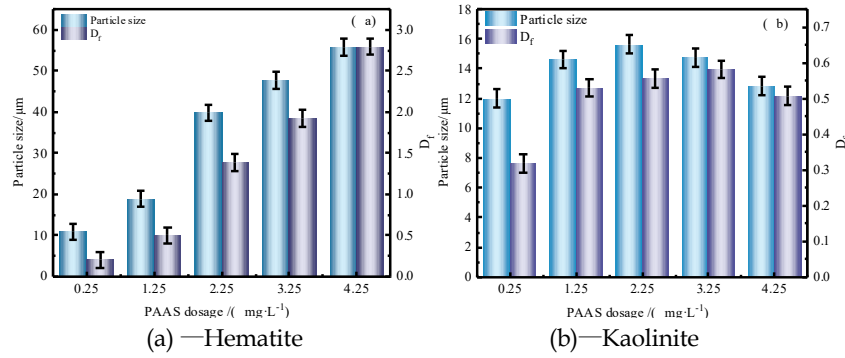


Fig. 8. Particle size and fractal dimension of flocs

Fig. 8(b) shows that the average particle size of kaolinite did not change significantly after interacting with PAAS, but it is larger than that of the original mineral. This is because kaolinite is a clay mineral and is more likely to stick together. The fractal dimension of kaolinite was overall smaller and did not change significantly, indicating that the kaolinite particles were basically not agglomerated after the addition of PAAS.

3.2. FTIR measurement

Fig. 9 shows the FTIR spectra of hematite and kaolinite before and after PAAS treatment. As shown in Fig. 9(a), the bands at approximately 563.19 cm⁻¹ and 472.54 cm⁻¹ represent the stretching and bending vibrations of Fe-OH and Fe-O, respectively (Chen et al., 2015). After treatment with PAAS, the new band around 1649.08 cm⁻¹ represents the stretching vibrations of -COO- from PAAS (Peng et al., 2024). Additionally, the stretching vibrations of -CH₂- in the alkyl chain appear at around 2952.91 cm⁻¹ and 2366.57 cm⁻¹, indicating the presence of RCOOH substances adsorbed on the hematite surface. The intensity of the -COO- and -CH₂- signals increased significantly after treatment with PAAS, suggesting that PAAS adsorbed on the hematite surface. The characteristic peaks of Fe-O and Fe-OH shifted to around 557.41 cm⁻¹ and 474.37 cm⁻¹, respectively. The formation of new bonds and changes in bond strength can be explained by the chemical adsorption of PAAS on the hematite surface.

Fig. 9 (b) shows the FTIR spectra of kaolinite before and after treatment with PAAS. As shown in Fig. 9 (b), a telescopic vibrational peak of the Si-O-Si skeleton in kaolinite appeared at 1641.36 cm⁻¹. After PAAS treatment, no new adsorption bands appeared in the FTIR spectra of kaolinite, and the characteristic peaks of kaolinite did not show any significant changes, indicating that PAAS acted on the surface of kaolinite through physical adsorption.

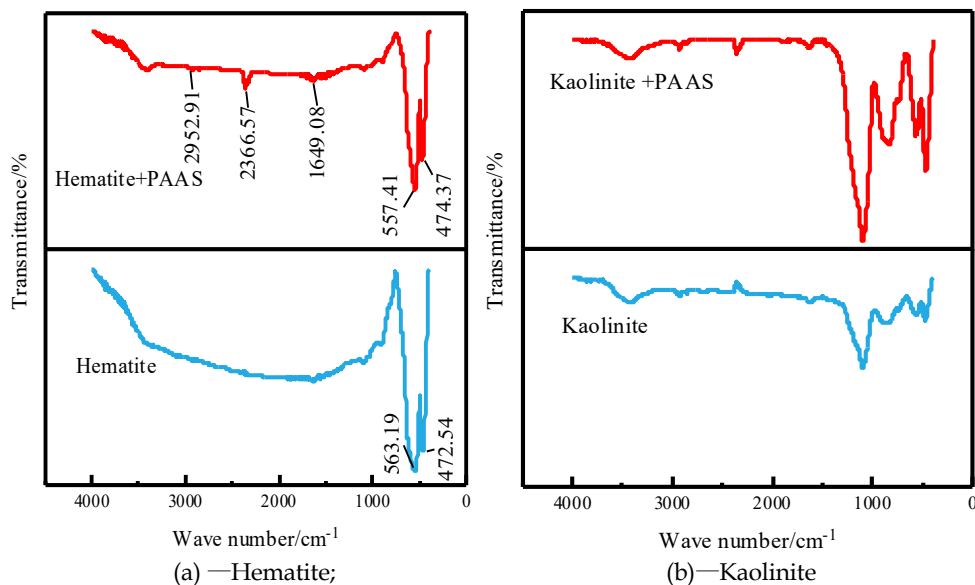


Fig. 9. The FTIR spectrum of PAAS

3.3. Zeta potential measurement

The degree of adsorption of different flotation chemicals on the mineral surface can be determined from the change in Zeta potential on the mineral particle surface. Fig. 10 shows the Zeta potential of the supernatants obtained with different doses of PAAS added to hematite and kaolinite. As shown in Fig. 10, the zeta potential of the supernatant of kaolinite was -7.80 mV under the condition of no addition of PAAS. After treating kaolinite with PAAS, the zeta potential decreased significantly with the increase in the dosage of PAAS, and reached a minimum of -15.9 mV at the dosage of PAAS of 4.25 $\text{mg}\cdot\text{L}^{-1}$. Without the addition of PAAS, the zeta potential of the hematite supernatant was -15.9 mV. Supernatant was -6.55 mV, and with the addition of PAAS, the zeta potential of hematite first moved in the positive direction, reaching a maximum of -3.53 mV at a PAAS dosage of 2.25 $\text{mg}\cdot\text{L}^{-1}$, and then decreased rapidly, reaching a minimum value of -11.8 mV at a PAAS dosage of 4.25 $\text{mg}\cdot\text{L}^{-1}$. From the relative change in zeta potential, the adsorption of PAAS on the hematite surface may reach a maximum at a PAAS dosage of 2.25 $\text{mg}\cdot\text{L}^{-1}$. Based on the chemical properties of the solution, it is reasonable to assume that the COO- or RCOO- component of PAAS may have a negative effect on the zeta potential.

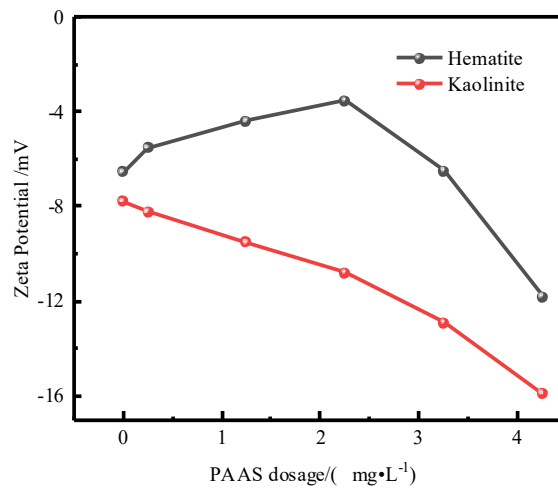


Fig. 10. Effect of PAAS on the zeta potential of hematite and kaolinite

3.4. Determination of PAAS adsorption on mineral surfaces

It is important to explore the adsorption phenomenon of flocculants on mineral surfaces during the flotation process, and the determination of the adsorption number of flocculants on hematite and kaolinite is a key indicator to evaluate whether the flocculants are effectively utilized. The amount of PAAS adsorbed per unit mass on hematite and kaolinite particles was determined by TOC analysis, and the observed adsorption data of PAAS on the surface of hematite and kaolinite are shown in Fig. 11.

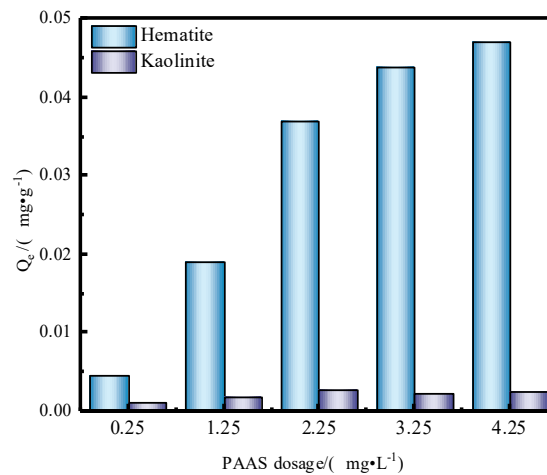


Fig. 11. Effect of PAAS dosage on the equilibrium amount (Q_e) of adsorbed PAAS.

According to Fig. 11, it can be seen that the amount of PAAS adsorbed on hematite particles increased with the increase of PAAS dosage, and the larger amount of PAAS adsorbed on hematite particles was $0.037 \text{ mg} \cdot \text{g}^{-1}$ when the PAAS dosage was $2.25 \text{ mg} \cdot \text{L}^{-1}$, and $0.037 \text{ mg} \cdot \text{g}^{-1}$ when the PAAS dosage was $4.25 \text{ mg} \cdot \text{L}^{-1}$, the PAAS adsorption on hematite particles reached a maximum value of $0.047 \text{ mg} \cdot \text{g}^{-1}$. Compared with hematite, the adsorption of PAAS on kaolinite was in a smaller range, and the maximum PAAS adsorption on kaolinite particles was $0.0027 \text{ mg} \cdot \text{g}^{-1}$ when the PAAS dosage was $2.25 \text{ mg} \cdot \text{L}^{-1}$. Compared with hematite, the adsorption of PAAS on kaolinite was in a smaller range, which was in agreement with the flocculation test results, PAAS is more easily adsorbed on the surface of hematite particles, has a stronger flocculation ability on hematite than quartz, and has a selective flocculation effect on hematite.

The Langmuir and Freundlich isotherm models were used to fit the experimental data for PAAS adsorption on hematite and kaolinite. The experimental data for the adsorption isotherms are shown in Figs. 12 and 13.

Different adsorption model parameters were introduced based on the fitted equations in Figs. 12 and 13 and combined with Eq. The specific data are shown in Tables 1 and 2.

From Table 1, it can be seen that the Langmuir model fits in descending order: hematite > kaolinite. The constant K_L is related to the adsorption capacity, and from K_L , PAAS has a stronger adsorption capacity under the mineral condition of hematite. For the Freundlich model it can be seen from Table 2 that the Freundlich model fits in the order from largest to smallest: hematite > kaolinite, and from the value of K_F , it can be seen that the adsorption of PAAS by hematite is better, while the adsorption of kaolinite is poorer.

Under the same experimental conditions, $R_L^2 > R_F^2$, indicating that the adsorption data of PAAS on hematite and kaolinite are more consistent with the Langmuir equation, and the adsorption of PAAS on hematite and kaolinite is monolayer adsorption.

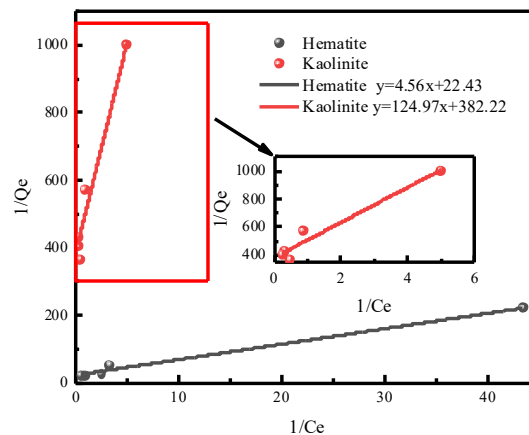


Fig. 12. Langmuir linear equation for isothermal adsorption of PAAS on hematite and kaolinite surfaces

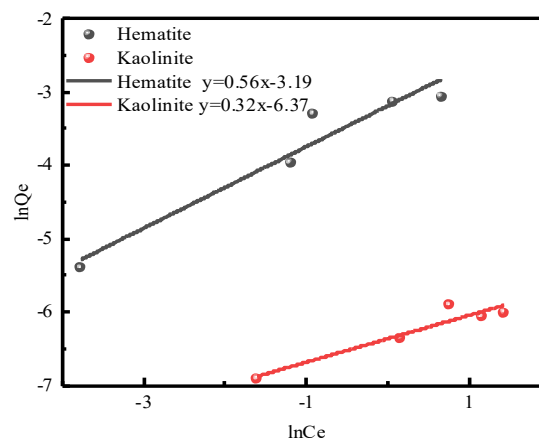


Fig. 13. Freundlich linear equation for isothermal adsorption of PAAS on hematite and kaolinite surfaces

Table 1. Langmuir fitting equations and parameters

minerals	Fitting equation	$K_A/(L \text{ mg}^{-1})$	$Q_m/(mg \text{ g}^{-1})$	R_L^2
Hematite	$y=4.56x+22.43$	4.91	0.0446	0.9898
Kaolinite	$y=124.97x+382.22$	3.06	0.0026	0.9538

Table 2. Freundlich fitting equations and parameters

minerals	Fitting equation	$K_F/(L \text{ mg}^{-1})$	n	R_F^2
Hematite	$y=0.56x-3.19$	0.0412	1.74	0.9377
Kaolinite	$y=0.32x-6.37$	0.0017	3.13	0.9020

3.5. XPS analysis

At a PAAS dosage of 2.25 mg L^{-1} , XPS analysis of the surface chemistry of hematite and the XPS results before and after hematite reacted with PAAS are shown in Fig. 14. As depicted in Fig. 14, peaks corresponding to Fe, C, and O binding energies were detected in the full spectrum of pure hematite after treatment with PAAS. Changes in the relative atomic concentrations on the surface of hematite are listed in Table 3. As shown in Table 3, after treatment with PAAS, the relative atomic concentrations of C 1s, O 1s, and Fe 2p were 62.26%, 34.13%, and 3.61%, respectively, indicating the adsorption of PAAS on the surface of hematite.

Fig. 15 shows the high-resolution XPS spectra and split-peak fitting results of C 1s and O 1s on the surface of hematite treated with sodium polyacrylate, respectively. As shown in Fig. 15(a), there are four binding energy peaks of 284.2 eV, 285.5 eV, 287.07 eV, and 288.3 eV in the C 1s peak fitting results of hematite, representing -CH, -CO, -C=O, and -COOH, respectively (Feng et al., 2016; Moreira et al., 2017; Zhang et al., 2019).

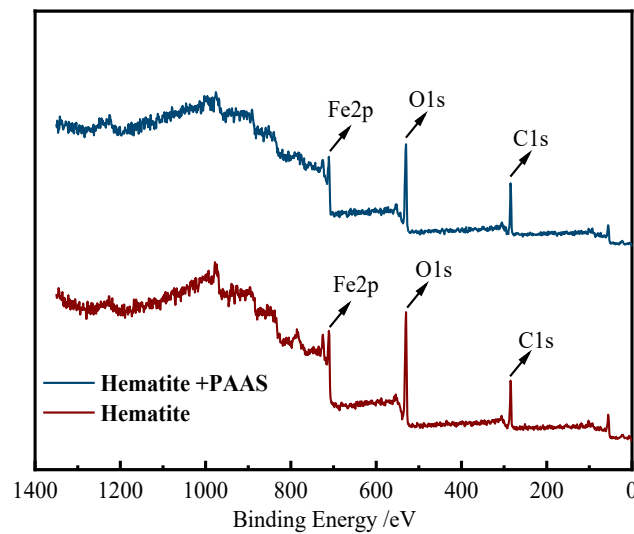


Fig. 14. XPS measured spectra of hematite before and after reaction with PAAS

Table 3. XPS measurements of hematite before and after reaction with PAAS

Category	Peak/eV	Half-height width/eV	Atomic concentration/%
Hematite	C1s	284.87	43.24
	O1s	531.4	44.92
	Fe2p	710.95	11.84
Hematite+PAAS	C1s	284.87	62.26
	O1s	531.4	34.13
	Fe2p	710.95	3.61

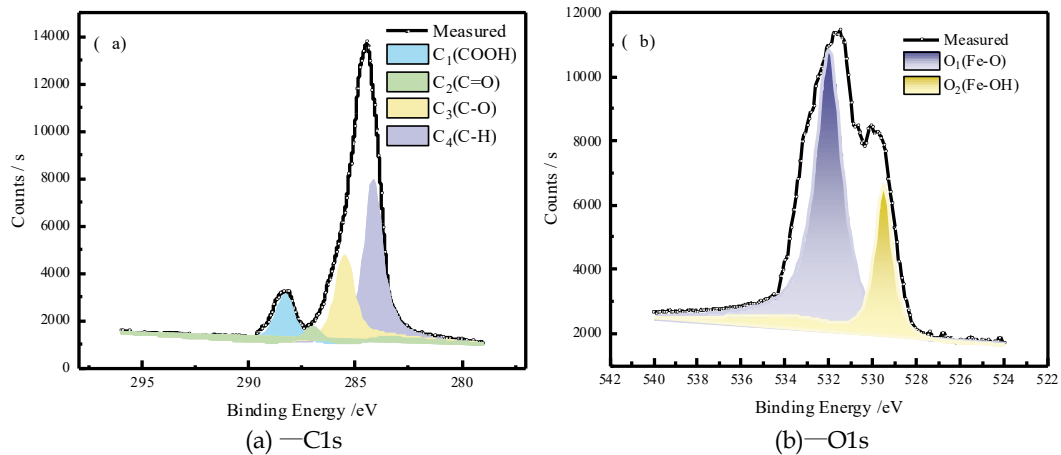


Fig. 15. High resolution XPS spectra of hematite after reaction with PAAS

Based on the above analysis, it can be seen that Fe-OH was generated on the hematite surface after the action of PAAS, and the high-resolution XPS spectra of O1s provided further evidence for this mechanism. Furthermore, -C=O and -COOH in PAAS were adsorbed on the surface of microfine-grained hematite by chemical interaction. After PAAS treatment, no new adsorption bands appeared in the FTIR spectra of kaolinite and the characteristic peaks of kaolinite showed slight changes, indicating that PAAS adsorbed on the surface of kaolinite by physical action. The mechanism is shown in Fig. 16.

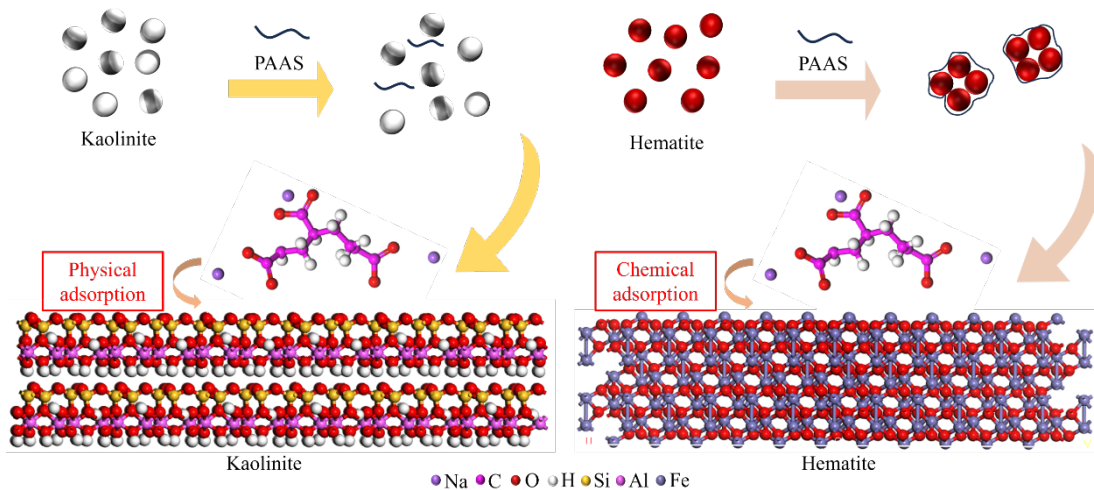


Fig. 16. Flocculation mechanism of PAAS on hematite and kaolinite surfaces

4. Conclusions

In this paper, the effect and difference of sodium polyacrylate on the selective flocculation of ultrafine hematite and kaolinite were investigated in detail using sodium polyacrylate, which is environmentally friendly, excellent in selectivity and harmless to the human body as a flocculant, and the selective flocculation of ultrafine hematite and kaolinite and its mechanism of action were revealed. The effect of sodium polyacrylate on the flocculation behavior of ultrafine hematite and kaolinite was revealed through flocculation test and floc particle size analysis, while XPS, FTIR, adsorption isothermal fitting calculations, and zeta potential test were used to reveal the mechanism of the action of sodium polyacrylate on hematite and kaolinite, which provides a new way of thinking for the reuse of the resources of the low-grade ultrafine iron tailings. The main conclusions of the study are as follows:

1. The flocculation test confirmed that the addition of 2.25 mg·L⁻¹ sodium polyacrylate (PAAS) increased the particle size of ultrafine hematite from 2.59 μm to 42.88 μm, with a fractal dimension of the flocculate reaching 1.59, indicating a relatively dense flocculate structure. The particle size and

- fractal dimension of kaolin showed no significant changes after the addition of PAAS, indicating that the addition of PAAS can selectively flocculate ultrafine hematite particles.
- FTIR analysis revealed that after treatment with PAAS, the intensity of the signals related to -COO- and -CH₂- significantly increased, indicating the adsorption of PAAS on the surface of ultrafine hematite particles. However, in the FTIR spectrum of kaolin, no new adsorption bands were observed, and the characteristic peaks of kaolin showed slight changes, indicating that PAAS adsorbed on the surface of kaolin via hydrogen bonding.
 - Results from zeta potential measurements, adsorption capacity, and XPS analysis demonstrate the strong adsorption capability of PAAS on the surface of hematite. Moreover, the adsorption data of PAAS on hematite and kaolin surfaces conform more closely to the Langmuir equation, indicating that the adsorption of PAAS on hematite and kaolin is monolayer adsorption.

Acknowledgments

This research was funded by the National Natural Science Foundation of China (Grant No.52374265), the Central Guided Local Science and Technology Development Funding Program (Grant No. 236Z4106G), the Natural Science Foundation of Hebei Province (Grant No. E2022209108), and Key Projects of Hebei Provincial Department of Education (Grant No. ZD2022059).

Reference

- LI, M., XIANG, Y., CHEN, T., GAO, X., LIU, Q., 2021. Separation of ultra-fine hematite and quartz particles using asynchronous flocculation flotation. *Minerals Engineering*. 164: 106817.
- ZHANG, M., XU, Z., ZHANG, Q., DAN, Z., FU, H., YAO, W., 2023. Properties and potential application of ozone-oxidized starch for enhanced reverse flotation of fine hematite. *Minerals Engineering*. 198: 108084.
- ZHU, Z. L., LI, Z., YIN, W. Z., YANG, B., ZHANG, N. N., QU, J. Z., CHEN, S. J., CHANG, J., YU, Y. X., LIU, L. J., 2022. Effect of surface roughness on the flotation separation of hematite from fine quartz. *Journal of Industrial and Engineering Chemistry*. 109: 431-441.
- WANG, L., HAO, X., YAO, J., YANG, B., 2023. Mechanism Study of Enhanced Hematite Reverse Flotation Desilication by Flocculation of Micro Fine Kaolinite with Polyoxyethylene Oxide. *Journal of Northeastern University(Natural Science)*. 44 (1): 110-116.
- MOCHIZUKI, Y., TSUBOUCHI, N., 2019. Removal of gangue components from low-grade iron ore by hydrothermal treatment. *Hydrometallurgy*. 190: 105159.
- CUI, F., MU, W., ZHAI, Y., GUO, X., 2020. The selective chlorination of nickel and copper from low-grade nickel-copper sulfide-oxide ore: Mechanism and kinetics. *Separation and Purification Technology*. 239: 116577.
- BAI, H., LIU, Y., ZHAO, Y., CHEN, T., LI, H., CHEN, L., SONG, S., 2020. Regulation of coal flotation by the cations in the presence of clay. *Fuel*. 271: 117590.
- ZHU, Z., YIN, W., YANG, B., FU, Y., XUE, J., 2019. Reduction of the slime contamination on fine coking coal by using the reverse-and-direct flotation process. *Colloids and Surfaces A Physicochemical and Engineering Aspects*. 579 (1): 123681.
- CHEN, X. AND PENG, Y., 2018. Managing clay minerals in froth flotation – A critical review. *Mineral Processing & Extractive Metallurgy Review*. 1-19.
- YANG, B., YIN, W., ZHU, Z., WANG, D., HAN, H., FU, Y., SUN, H., CHU, F., YAO, J., 2019. A new model for the degree of entrainment in froth flotation based on mineral particle characteristics. *Powder Technology*. 354: 358-368.
- YU, Y., LI, A., XU, Z., ZHOU, A., LI, Z., ZHANG, N., QU, J., ZHU, X., LIU, Q., 2020. New insights into the slime coating caused by montmorillonite in the flotation of coal. *Journal of Cleaner Production*. 242: 118540.
- FARROKHPAY, S., NDLOVU, B., BRADSHAW, D., 2016. Behaviour of swelling clays versus non-swelling clays in flotation. *Minerals Engineering*. 96-97: 59-66.
- LI, C., RUNGE, K., SHI, F., FARROKHPAY, S., 2016. Effect of flotation froth properties on froth rheology. *Powder Technology*. 294: 55-65.
- WANG, Z., MU, Y., ZHANG, M., CAO, Y., LI, C., 2024. Effect of clay crystal structure on froth rheology in flotation. *Powder Technology*. 435: 119395.
- WARREN, L. J., 1975. Shear-flocculation of ultrafine scheelite in sodium oleate solutions. *Journal of Colloid and Interface Science*. 50 (2): 307-318.
- FORBES, E., 2011. Shear, selective and temperature responsive flocculation: A comparison of fine particle flotation techniques. *International Journal of Mineral Processing*. 99 (1): 1-10.

- YIN, W.-Z., YANG, X.-S., ZHOU, D.-P., LI, Y.-J., LÜ, Z.-F., 2011. *Shear hydrophobic flocculation and flotation of ultrafine Anshan hematite using sodium oleate*. *Transactions of Nonferrous Metals Society of China*. 21 (3): 652-664.
- BAI, S., LI, J., BI, Y., YUAN, J., WEN, S., DING, Z., 2023. *Adsorption of sodium oleate at the microfine hematite/aqueous solution interface and its consequences for flotation*. *International Journal of Mining Science and Technology*. 33 (1): 105-113.
- WANG, Y., WEI, D., QIN, W., JIAO, F., LUO, X., PAN, Z., 2023b. *Effect of nanobubbles on particle flocculation in sodium oleate-calcite flotation system*. *Minerals Engineering*. 204: 108438.
- YANG, S., ZHANG, H., CHI, R., BAO, S., XU, Y., LIU, C., 2023. *A critical review on the application of green polymer-type scale inhibitors in mineral flotation*. *Minerals Engineering*. 204: 108436.
- RAJU, G. B., SUBRAHMANYAM, T. V., SUN, Z., FORSLING, W., 1991. *Shear-flocculation of quartz*. *International Journal of Mineral Processing*. 32 (3): 283-294.
- PASCOE, R. D., WILLS, B. A., 1994. *Selective aggregation of ultrafine hematite and quartz under high shear conditions with conventional flotation collectors*. *Minerals Engineering*. 7 (5): 647-656.
- AKDEMİR, Ü., 1997. *Shear flocculation of fine hematite particles and correlation between flocculation, flotation and contact angle*. *Powder Technology*. 94 (1): 1-4.
- PAVLOVIC, S., BRANDAO, P. R. G., 2003. *Adsorption of starch, amylose, amylopectin and glucose monomer and their effect on the flotation of hematite and quartz*. *Minerals Engineering*. 16 (11): 1117-1122.
- RULYOV, KOROLYOV, KOVALCHUK, 2009. *Ultra flocculation of quartz suspensions: effects of shear rate, particle size distribution and solids content*. *Mineral Processing and Extractive Metallurgy*. 118 (3): 175-181.
- XIE, Y., YIN, W., YAO, J., XUE, F., LIU, J., BAN, X., 2024. *Application and mechanism of an efficient hydrophobic flocculant CPAM in the flocculation reverse flotation of hematite and microfine-grained chlorite*. *Journal of Environmental Chemical Engineering*. 12 (3): 112608.
- YANG, C., LI, M. Y., LONG, H. M., H.C.WANG, Q.LIU, 2022. *Study on asynchronous flocculation flotation separation of fine quartz/hematite*. *Mineral protection and utilization*. 42 (05): 82-87.
- HAN, Y. Q., YANG, Z. C., TENG, Q., ZHANG, G. Y., FANG, S. H., ZHANG, S. H., LIU, S. Y., 2024. *Fe (III) -XG Complex Selective Flocculation of Fine-grained Hematite and Quartz and Its Mechanism*. *Nonferrous metals (Mineral Processing Section)*. (01): 116-125.
- CHEN, Z. Q., ZHEN, M. Y., PENG, T. F., 2022. *The influence of sodium polyacrylate on the flotation of serpentine and its mechanism*. *Multipurpose utilization of mineral resources*. (02): 100-104.
- CHENG, K., WU, X., TANG, H., ZENG, Y., 2022. *The flotation of fine hematite by selective flocculation using sodium polyacrylate*. *Minerals Engineering*. 176: 107273.
- CHEN, X., HU, H., LIU, J., CHEN, H., WANG, Q., 2015. *Flocculation performance and mechanism of hydroxamate flocculants on synthetic hematite or goethite suspension*. *Journal of Central South University*. 22 (05): 1626-1634.
- PENG, J., ZHENG, Y., WANG, Z., DAI, Z., GUO, Z., 2024. *Study on the surface activation of ilmenite by persulfate and flotation response*. *Separation and Purification Technology*. 343: 127079.
- FENG, Q., WEN, S., ZHAO, W., DENG, J., XIAN, Y., 2016. *Adsorption of sulfide ions on cerussite surfaces and implications for flotation*. *Applied Surface Science*. 360: 365-372.
- MOREIRA, G. F., PEÇANHA, E. R., MONTE, M. B. M., LEAL FILHO, L. S. AND STAVALE, F., 2017. *XPS study on the mechanism of starch-hematite surface chemical complexation*. *Minerals Engineering*. 110: 96-103.
- ZHANG, N., EJTEMAEI, M., NGUYEN, A. V., ZHOU, C., 2019. *XPS analysis of the surface chemistry of sulfuric acid-treated kaolinite and diasporite minerals with flotation reagents*. *Minerals Engineering*. 136: 1-7.